



Contents lists available at ScienceDirect

International Journal of Heat and Mass Transfer

journal homepage: www.elsevier.com/locate/ijhmt

Microwave heating of saturated packed bed using a rectangular waveguide (TE₁₀ mode): Influence of particle size, sample dimension, frequency, and placement inside the guide

W. Klinbun, P. Rattanadecho*, W. Pakdee

Research Center of Microwave Utilization in Engineering (R.C.M.E.), Department of Mechanical Engineering, Faculty of Engineering, Thammasat University (Rangsit Campus), Pathumthani 12120, Thailand

ARTICLE INFO

Article history:

Received 23 May 2010

Received in revised form 10 December 2010

Available online 18 February 2011

Keywords:

Microwave heating
Saturated packed bed
Rectangular waveguide
TE₁₀ mode

ABSTRACT

This paper presents the numerical and experimental analysis of microwave heating in a saturated packed bed by using a rectangular waveguide (TE₁₀ mode). A complete mathematical model is proposed, which uses comprehensive two-dimensional energy and momentum equations to describe unsteady temperature and flow fields, coupled with a complete solution of the transient Maxwell's equations in time domain. The influences of particle size, sample dimension, placement inside the guide, and frequency on heat transfer and flow pattern are studied. The simulation results are in good agreement with experimental data. Flow pattern strongly depends on the bead size and thermal efficiency of the sample changes with sample size and frequency. Furthermore, the middle placed inside the guide aids in uniform heating.

© 2011 Elsevier Ltd. All rights reserved.

1. Introduction

Microwave technology is widely implemented in industrial processes such as heating, drying, melting, and pasteurizing [1]. Since microwave radiation can penetrate into material directly and is heated up by polarization mechanism that occurs millions of times per second, that results in short process time, high thermal efficiency and lower waste. Various types of porous medium occur in many industries such as wood, food, ceramic and concrete. Porous medium is a material that consists of a solid matrix with an interconnected void [2]. Previous investigations of heating porous medium have appeared in the recent literature [3–9]. Almost previous attentions are paid on the momentum and energy transfer in cavity filled with a porous medium subjected to prescribed temperature and wall heat flux conditions. The natural or free convection in a porous medium has been studied extensively. However, previous works concerning microwave heating of porous medium in case of without phase change and with phase change are as follows: Chen Kou et al. [10] proposed model for predicting local moisture content, as densities and pressure. Rattanadecho et al. [11] studied the influence of particle size and initial moisture content on each driving forced mechanism (vapor diffusion and capillary flow) during microwave drying process of an unsaturated porous material. From the results, the small bead size led to much higher capillary forces resulting in a faster drying time. Rattanadecho

[12] investigated the drying of wood using a rectangular waveguide. The results showed that the simulations are performed illustrating the influence of irradiation times, working frequencies and sample size. Cha-um et al. [13] studied experimentally the heating process of dielectric materials by microwave with a rectangular waveguide. This work investigated the effects of the microwave power level, type of sample, dimension, and placement inside the guide. The results showed that the placement of sample inside the waveguide is greatly affected by temperature and power absorbed within the material than the other parameters.

For multiphase system and food sample, Ni et al. [14] developed a multiphase porous media model to predict moisture transport during intensive microwave heating of biomaterials. Internal pressure gradients arose from internal heating and vaporization significantly enhance the transport. The hot air and/or infrared heating of the surface to increase evaporation were suggested as ways to reduce surface moisture build-up. Dinčov et al. [15] presented the numerical results for the intensive microwave heating of multi-phase porous materials. The model showed moisture movement results from internal pressure gradients produced by the internal heat generation due to microwave energy. Basak and Meenakshi [16] investigated the effect of ceramic supports (Al₂O₃, SiC) on microwave heating of composite dielectric food slabs. Al₂O₃ support may cause thermal runaway whereas SiC support may reduce the thermal runaway, based on suitable distribution of microwaves supplied at the both sides. Zhang et al. [17] studied the microwave sterilization of solid foods using numerical modeling and experimental work. Heating patterns

* Corresponding author. Tel.: +662 564 3001x3153; fax: +662 564 3010.

E-mail address: ratphadu@engr.tu.ac.th (P. Rattanadecho).

Nomenclature

C_p	specific heat capacity (J/kg K)	η	dynamic viscosity (Pa s)
E	electric field intensity (V/m)	κ	permeability (m ²)
f	frequency of incident wave (Hz)	λ	wavelength (m)
g	gravitational constant (m/s ²)	μ	magnetic permeability (H/m)
H	magnetic field intensity (A/m)	ν	kinematics viscosity (m ² /s)
P	power (W)	ρ	density (kg/m ³)
p	pressure (Pa)	σ	electric conductivity (S/m)
Q	local electromagnetic heat generation term (W/m ³)	v	velocity of propagation (m/s)
s	Poynting vector (W/m ²)	ω	angular frequency (rad/s)
T	temperature (°C)	ξ	surface tension (N/m)
t	time (s)		
$\tan \delta$	dielectric loss coefficient (-)	Subscripts	
u, w	velocity component (m/s)	∞	ambient condition
Z_H	wave impedance (Ω)	a	air
Z_I	intrinsic impedance (Ω)	in	input
		p	particle
Greek letters		r	relative
α	thermal diffusivity (m ² /s)	w	water
β	coefficient of thermal expansion (1/K)	x, y, z	coordinate
ε	permittivity (F/m)		
ϕ	porosity (-)		

changed qualitatively with geometry (shape and size) and properties (composition) of the food material, but optimal heating was possible by choosing suitable combinations of these factors.

The recent work of a microwave process combined with hot air and infrared to dry porous material is reported by Salagnac et al. [18]. They presented the numerical modeling of the hygrothermal behavior of a rectangular-shaped porous material during combined drying. The temperature, moisture content, and pressure fields were displayed in detail. The comparison between simulated results and experimental data results on cellular concrete showed the relevance of this model for studied on combined drying.

As a literature above, the previous works in the microwave field considered only the effect of parameters on heat and mass transport. Indeed, a little effort has been reported on the study of a fluid flow and heat transfer in a porous medium induced by microwave energy using a rectangular waveguide, especially a complete comparison between predicted results and experimental data. In addition, due to the limited amount of theoretical and experimental work on microwave heating of porous media such as packed bed of glass beads reported to date, the various effects are not fully understood and numbers of critical issues remain unresolved. The effects of the particle size, sample dimension, placement inside a waveguide and working frequencies on electric field distribution, flow and heating pattern have not been systematically studied.

The current study extended from Cha-um et al. [13]. It has been investigated theoretically and experimentally on microwave heating of a saturated packed bed using a rectangular waveguide (TE₁₀ mode). This work used the rectangular waveguide as an applicator because it is easy to handling electromagnetic fields in the system, thus the process can be simulated precisely. Microwave power input is 300 W. A saturated packed bed consists of single sized glass beads with only water in voids. The effects of particle sizes (diameters are 0.15 mm and 0.40 mm), sample sizes (full load and partial load), placement inside the guide (s_0 and s_{20}) and operating frequencies (1.5, 2.45 and 5.8 GHz) on electric field distribution, temperature profile and a flow pattern are investigated. The results presented here provide a basis for fundamental understanding of microwave heating of the saturated porous medium.

2. Experiment setup

Fig. 1 shows the experiment apparatus of microwave heating of saturated porous medium using a rectangular waveguide. The microwave system is a monochromatic wave of TE₁₀ mode operating at a frequency of 2.45 GHz. From Fig. 1(b), magnetron (no. 1) generates microwave and transmits along the z-direction of the rectangular waveguide (no. 5) with inside dimensions of 109.22 × 54.61 mm² toward to a testing area (red¹ circle) and a water load (no. 8) that is situated at the end of the waveguide. On the upstream side of the sample, an isolator is used to trap any microwave reflected from the sample to prevent damaging to the magnetron. The powers of incident, reflected and transmitted waves are measured by a wattmeter using a directional coupler (no. 6) (MICRO DENSHI., model DR-5000). Fiberoptic (no. 7) (LUXTRON Fluoroptic Thermometer, model 790, accurate to ±0.5 °C) is employed for temperature measurement. The fiberoptic probes are inserted into the sample, and situated on the x-z plane at $y = 25$ mm. (as seen in Fig. 1(c) and (d)) Due to the symmetrical condition, temperatures are measured for only one side of plane. The samples are saturated packed beds that compose of glass beads and water. Two sizes of glass bead, fine beads with diameter of 0.15 mm and coarse beads with diameter of 0.40 mm, are chosen to investigation in this work. A container is made from polypropylene which does not absorb microwave energy with a thickness of 0.75 mm.

3. Mathematical modeling

Fig. 2(a) and (b) shows the placement of sample inside a rectangular waveguide. There are s_0 and s_{20} where s_0 and s_{20} are position that is far from the center line of the waveguide 0 and 20 mm, respectively. Fig. 2(c) and (d) shows the computational domain of the problem in case of full and partial load, respectively. The case of full load is the condition in which the saturated packed bed cross-sectional area with a dimension of 54.61 × 109.22 mm²

¹ For interpretation of color in Fig. 1, the reader is referred to the web version of this article.

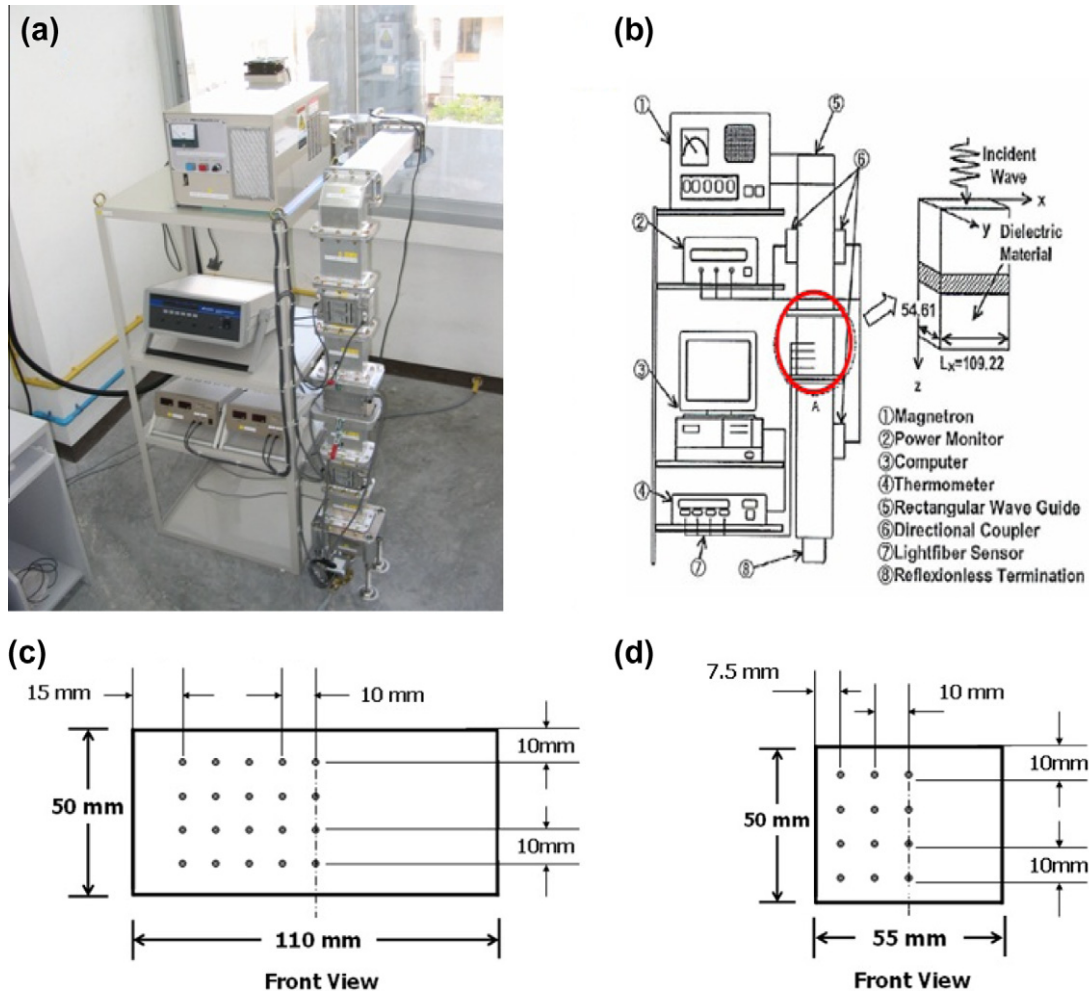


Fig. 1. Experiment setup; (a) picture; (b) diagram; (c, d) position of fiberoptic probes inside sample.

fitted in the waveguide, while partial load corresponds to saturated packed bed with a half cross-sectional area with dimension of $54.61 \times 54.61 \text{ mm}^2$. Inside the waveguide, a saturated glass beads is packed in a polypropylene container, whose all walls are insulated except the top surface.

3.1. Dielectric properties and penetration depth

Since the dielectric properties of a packed bed depend on the functional temperature. The theory surrounding mixing formulas is used throughout in this study, in which the volume fractions of water and glass bead are considered as follows [11]:

$$\epsilon_r(T) = \epsilon'_r(T) - j\epsilon''_r(T) \quad (1)$$

where

$$\epsilon'_r(T) = \phi\epsilon'_{rw}(T) + (1 - \phi)\epsilon'_{rp} \quad (2)$$

$$\epsilon''_r(T) = \phi\epsilon''_{rw}(T) + (1 - \phi)\epsilon''_{rp} \quad (3)$$

The loss tangent coefficient can be written as:

$$\tan \delta = \frac{\epsilon''_r(T)}{\epsilon'_r(T)} \quad (4)$$

When the material is heated unilaterally, it is found that as the dielectric constant and loss tangent coefficient vary, the penetration depth and the electric field within the dielectric material

varies. The penetration depth is used to denote the depth at which the power density has decreased to 37% of its initial value at the surface [12]

$$D_p = \frac{1}{\frac{2\pi f}{v} \sqrt{\frac{\epsilon'_r \left(\sqrt{1 + \left(\frac{\epsilon''_r}{\epsilon'_r}\right)^2} - 1 \right)}{2}}} = \frac{1}{\frac{2\pi f}{v} \sqrt{\frac{\epsilon'_r (\sqrt{1 + (\tan \delta)^2} - 1)}{2}}} \quad (5)$$

where D_p is penetration depth, ϵ''_r is relative dielectric loss factor. And v is microwave speed. The penetration depth of the microwave power is calculated according to Eq. (5), which shows how it depends on the dielectric properties of the material. It is noted that products with huge dimensions and high loss factors, may occasionally overheat a considerably thick layer on the outer layer. To prevent such phenomenon, the power density must be chosen so that enough time is provided for the essential heat transfer between boundary and core. If the thickness of the material is less than the penetration depth, only a fraction of the supplied energy will become absorbed. In example, consider the dielectric properties of water typically show moderate lossiness depending on the temperature. The water layer at low temperature typically shows slightly greater potential for absorbing microwaves. In the other words, an increase in the temperature typically decreases ϵ''_r , accompanied by a slight increase in D_p .

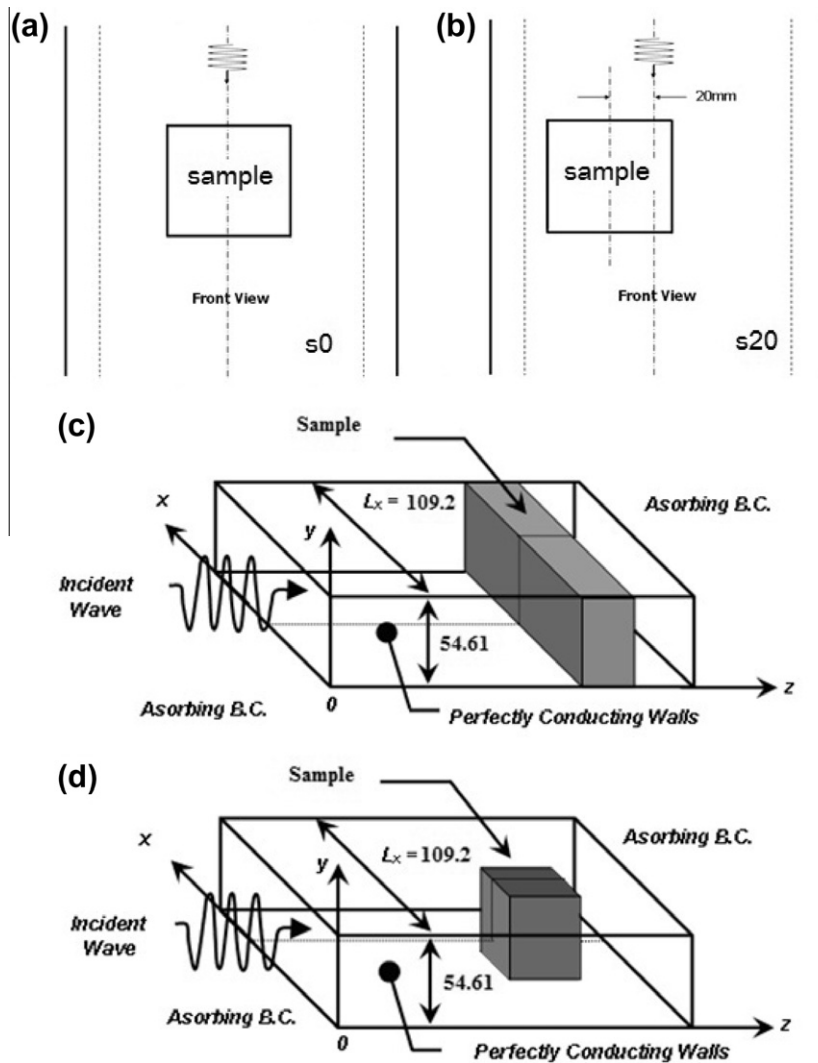


Fig. 2. (a, b) Placement of sample inside a rectangular waveguide; (c, d) computational domain of the problem.

3.2. Analysis of electromagnetic field

Since an investigated electromagnetic field is in the TE₁₀ mode, there is no variation of field in the direction between the broad faces of the rectangular waveguide and is uniform in the y-direction. Consequently, it is assumed that two dimensional model in x and z directions would be sufficient to identify the microwave heating phenomena in a rectangular waveguide [11]. The other assumptions are as follows:

- (1) The absorbed energy by air in a rectangular waveguide is negligible.
- (2) The walls of the rectangular waveguide are perfect conductors.
- (3) All materials are non-magnetic.
- (4) The effect of sample container on the electromagnetic can be neglected.

Maxwell's equations are solved for distribution of electromagnetic field inside the rectangular waveguide. For TE₁₀ mode, that is $E_x = E_z = H_y = 0$. Thus, Maxwell's equations can be written as [11]:

$$\varepsilon \frac{\partial E_y}{\partial t} = \frac{\partial H_x}{\partial z} - \frac{\partial H_z}{\partial x} - \sigma E_y \quad (6)$$

$$\mu \frac{\partial H_z}{\partial t} = -\frac{\partial E_y}{\partial x} \quad (7)$$

$$\mu \frac{\partial H_x}{\partial t} = \frac{\partial E_y}{\partial z} \quad (8)$$

where E and H denote electric field intensity and magnetic field intensity, respectively. ε is the electrical permittivity, σ is the electrical conductivity and μ is the magnetic permeability. These symbols are

$$\varepsilon = \varepsilon_0 \varepsilon_r \quad (9)$$

$$\mu = \mu_0 \mu_r \quad (10)$$

$$\sigma = 2\pi f \varepsilon \tan \delta \quad (11)$$

In addition, if magnetic effects are negligible, which is proven to be a valid assumption for most dielectric materials used in microwave heating applications, the magnetic permeability (μ) is well approximated by its value (μ_0) in the free space.

The boundary conditions for TE₁₀ mode can be formulated as follows:

- (1) Perfectly conducting boundaries. Boundary conditions on the inner wall surface of the waveguide are given by Faraday's law and Gauss's theorem:

$$E_t = 0, \quad H_n = 0 \quad (12)$$

where t and n are denoted tangential and normal direction, respectively.

- (2) Continuity boundary condition. Boundary conditions along the interface between sample and air are given by Ampere's law and Gauss's theorem:

$$E_t = E'_t, \quad H_t = H'_t \quad (13)$$

- (3) Absorbing boundary condition. At both ends of the rectangular waveguide, the first order absorbing conditions are applied [21]:

$$\frac{\partial E_y}{\partial t} = \pm v \frac{\partial E_y}{\partial z} \quad (14)$$

where \pm is represented forward and backward direction and v is velocity of the wave.

- (4) Oscillation of the electric and magnetic intensities by the magnetron. For incident waves due to magnetron are given by Ratanadecho et al. [11]:

$$E_y = E_{yin} \sin\left(\frac{\pi x}{L_x}\right) \sin(2\pi ft) \quad (15)$$

$$H_x = \frac{E_{yin}}{Z_H} \sin\left(\frac{\pi x}{L_x}\right) \sin(2\pi ft) \quad (16)$$

where E_{yin} is the input value of electric field intensity, L_x is the length of the rectangular waveguide in the x -direction, Z_H is the wave impedance defined as

$$Z_H = \frac{\lambda_g Z_l}{\lambda} = \frac{\lambda_g}{\lambda} \sqrt{\frac{\mu}{\epsilon}} \quad (17)$$

Here Z_l is intrinsic impedance depending on the properties of the material, λ and λ_g are the wave lengths of microwaves in free space and rectangular waveguide, respectively.

The power flux associated with a propagating electromagnetic wave is expressed by the Poynting vector:

$$s = \frac{1}{2} \text{Re}(E \times H^*) \quad (18)$$

The Poynting theorem allows the evaluation of the microwave power input. It is represented as

$$P_{in} = \int_A S dA = \frac{A}{4Z_H} E_{yin}^2 \quad (19)$$

3.3. Analysis of temperature profile and flow field

The analytical model is shown in Fig. 2(c) and (d). To reduce complexity of the problem, several assumptions have been offered into the flow and heat transfer analysis.

- (1) Corresponding to electromagnetic field, considering flow and temperature field can assume to be two-dimensional plane (x - z).
- (2) The saturated porous packed bed is rigid; no chemical reactions take place in this packed bed.
- (3) Local thermodynamic equilibrium is assumed.

The governing equations describing the heat transfer phenomenon are given by Pakee and Rattanadecho [9]:

$$\Phi \frac{\partial T}{\partial t} + u \frac{\partial T}{\partial x} + w \frac{\partial T}{\partial z} = \alpha \left(\frac{\partial^2 T}{\partial x^2} + \frac{\partial^2 T}{\partial z^2} \right) + \frac{Q}{(\rho C_p)_w} \quad (20)$$

where Φ is heat capacity ratio, the equation is given as

$$\Phi = \frac{\phi(\rho C_p)_w + (1 - \phi)(\rho C_p)_p}{(\rho C_p)_w} \quad (21)$$

where Q is the local electromagnetic heat generation term, which is a function of the electric field, dielectric loss factor and frequency, and can define as

$$Q = \omega \epsilon_0 \epsilon_r'' E^2 = 2\pi \cdot f \cdot \epsilon_0 \cdot \epsilon_r' (\tan \delta) E_y^2 \quad (22)$$

The governing equations describing the fluid flow phenomena are the system of momentum equations. This form of momentum equation is known as Brinkmann-extended Darcy model [9] where the Brinkmann term describes viscous effects due to the presence of solid body.

Continuity equation

$$\frac{\partial u}{\partial x} + \frac{\partial w}{\partial z} = 0 \quad (23)$$

Momentum equations

$$\frac{1}{\phi} \left(\frac{\partial u}{\partial t} \right) + \frac{1}{\phi^2} \left(u \frac{\partial u}{\partial x} + w \frac{\partial u}{\partial z} \right) = -\frac{1}{\rho_w} \left(\frac{\partial p}{\partial x} \right) + \frac{v}{\phi} \left(\frac{\partial^2 u}{\partial x^2} + \frac{\partial^2 u}{\partial z^2} \right) - \frac{uw}{\kappa} \quad (24)$$

$$\frac{1}{\phi} \left(\frac{\partial w}{\partial t} \right) + \frac{1}{\phi^2} \left(u \frac{\partial w}{\partial x} + w \frac{\partial w}{\partial z} \right) = -\frac{1}{\rho_w} \left(\frac{\partial p}{\partial z} \right) + \frac{v}{\phi} \left(\frac{\partial^2 w}{\partial x^2} + \frac{\partial^2 w}{\partial z^2} \right) - \frac{vw}{\kappa} + g\beta(T - T_\infty) \quad (25)$$

where κ is medium permeability, β is thermal expansion coefficient, α is effective thermal diffusivity of the porous medium, v is kinetic viscosity of the fluid. In the present study, the heat capacity ratio Φ is taken to be unity since the thermal properties of the solid matrix and the fluid are assumed to be identical.

Boundary and initial conditions for analysis of temperature profile and flow field:

- (1) The upper surface can exchange with surrounding, so that heat is lost from the surface via natural convection:

$$-\lambda \frac{\partial T}{\partial z} = h_c(T - T_\infty) \quad (26)$$

where h_c is the local heat transfer coefficient.

The velocity in the normal direction (w) and shear stress in the horizontal direction are assumed to be zero, where the influence of Marangoni flow can be applied [19]:

$$\eta \frac{\partial u}{\partial z} = -\frac{d\xi}{dT} \frac{\partial T}{\partial x} \quad (27)$$

where η and ξ are the dynamic viscosity and surface tension of liquid layer, respectively.

- (2) The walls, except the upper surface, are insulated. Furthermore, the container is rigid body, zero slip boundary conditions are applied for the momentum equations

$$\frac{\partial T}{\partial x} = \frac{\partial T}{\partial z} = 0 \quad (28)$$

- (3) The initial condition for microwave heating process is defined as:

$$T = T_0 \quad \text{at } t = 0 \quad (29)$$

4. Numerical procedures

The description of heat transport and flow pattern, Eqs. (20)–(25) requires specification of temperature (T), velocities components

(u, w) and pressure (p). These equations are coupled to the Maxwell's equations (Eqs. (6)–(8)) by Eq. (21). It represents the heating effect of the microwaves in the packed bed-container domain. The electromagnetic equations are solved by using Finite difference time domain (FDTD) method. With this method, the electric field components (E) are stored halfway between the basic nodes while magnetic field components (H) are stored at the center. Hence, they are calculated at alternating half-time steps. E and H field components are discretized by a central difference method (second-order accurate) in both spatial and time domain.

Spatial and temporal resolution is selected to ensure of stability and accuracy. To insure stability of the time-stepping algorithm Δt is chosen to satisfy the courant stability condition [11]:

$$\Delta t \leq \frac{\sqrt{(\Delta x)^2 + (\Delta z)^2}}{v} \quad (30)$$

And the spatial resolution of each cell defines as:

$$\Delta x, \Delta z \leq \frac{\lambda_g}{10\sqrt{\epsilon_r}} \quad (31)$$

Corresponding to Eqs. (30) and (31), the calculation conditions are as follows: $\Delta x = 1.0922$ mm, $\Delta z = 1.0000$ mm, and $\Delta t = 2 \times 10^{-12}$ s.

Eqs. (20)–(25) are solved numerically by using the finite control volume (FCV) method with the SIMPLE algorithm developed by Patankar [20]. The reason to use this method is advantages of flux conservation that avoids generation of parasitic source. The basic strategy of the finite control volume discretization method is to divide the calculated domain into a number of control volumes and then integrate the conservation equations over this control volume over an interval of time $[t, t + \Delta t]$. At the boundaries of the calculated domain, the conservation equations are discretized by integrating over half the control volume and taking into account the boundary conditions. At the corners of the calculated domain used a quarter of control volume. The fully implicit time discretization finite difference scheme is used to arrive at the solution in time. The time step is $\Delta t = 0.01$ s and relative error in the iteration procedures of 10^{-6} is chosen. Additionally, the details about numerical discretization of this method can be found in the recent literatures.

Table 1
The electromagnetic and thermophysical properties used in the computations.

Property	Air	Water	Glass bead
Heat capacity, C_p ($\text{J kg}^{-1} \text{K}^{-1}$)	1007	4190	800
Thermal conductivity, λ ($\text{W m}^{-1} \text{K}^{-1}$)	0.0262	0.609	0.14
Density, ρ (kg m^{-3})	1.205	1000	2500
Dielectric constant, ϵ_r'	1.0	$88.15 - 0.414T + (0.131 \times 10^{-2})T^2 - (0.046 \times 10^{-4})T^3$	5.1
Loss tangent, $\tan \delta$	0.0	$0.323 - (9.499 \times 10^{-3})T + (1.27 \times 10^{-4})T^2 - (6.13 \times 10^{-7})T^3$	1.0

Table 2
Dielectric properties of porous packed bead ($T = 28$ °C).

Frequency (GHz)	1.5		2.45		5.8	
	0.15	0.40	0.15	0.40	0.15	0.40
Dielectric constant, ϵ_r'	32.9678	32.2440	32.9678	32.2440	32.9678	32.2440
Loss factor, ϵ_r''	2.0195	1.9322	2.0195	1.9322	2.0195	1.9322
Penetration depth (m)	0.1810	0.1870	0.1102	0.1145	0.0468	0.0483

5. Results and discussion

The experimental data for microwave heating of the porous packed bed are compared with the predicted results. The packed beds with initial temperature of 28 °C are used for the present analysis. The dielectric and thermal properties of water, air and glass bead are listed in Table 1. The penetration depth of porous packed bed is calculated by Eq. (5) and the values are listed in Table 2. The characteristic of water transport in porous material are shown in Table 3.

The results are divided into four parts including the effects of particle sizes, sample sizes, sample positions inside a waveguide and microwave frequency on electric field distribution, temperature profile and a flow pattern.

5.1. The effect of particle sizes

The results of the effect of particle size on microwave heating phenomena for specified heating conditions; $P = 300$ W, $f = 2.45$ GHz, $t = 60$ s and sample size = 109.2 mm (x : width) \times 50 mm (z : depth) are presented as follows.

Fig. 3 shows the simulation of electric field distributions of TE₁₀ mode inside a rectangular waveguide when sample is inserted inside the waveguide. In Fig. 3, vertical axis represents the intensity of electric field E_y , which is normalized to the amplitude of the input electric field, $E_{y,in}$. It reveals that a stronger standing wave with a larger amplitude forms in the cavity forward to the sample while the electric field within the sample is extinguished. Since the incident wave passing through the cavity having low permittivity is directly irradiated to the sample having high permittivity, the major part of incident wave is reflected and resonated while other part that is a minor part is transmitted. A water layer (Fig. 3(a)) is high lossy material but the packed bed is low lossy material (Fig. 3(b) and (c)). In case of the high lossy material, the transmitted waves are almost absorbed at the leading edge of the sample. While the transmitted waves in case of the low lossy material will reflect from the bottom surface and resonate with transmitted waves inside material. So electric field amplitude within the packed bed is higher. The comparison of the electric field distribution between the packed beds which have the particle size of 0.15 and 0.40 mm are shown in Fig. 3(b) and (c), respectively. The two cases reveal a similar profile with a little different in magnitude.

Temperature profiles within the samples at $t = 60$ s are shown in Fig. 4. From the results, temperature profile of a water layer is quite different from the temperature profile of the packed beds due to the different in its dielectric and hydrodynamic properties. There appear good agreements with electric field distribution. In Fig. 4, temperature is high at the center of the sample due to the

Table 3
The characteristic of water transport in porous material.

Diameter, d (mm)	Porosity, ϕ (-)	Permeability, κ (m^2)
0.15	0.385	8.41×10^{-12}
0.40	0.371	3.52×10^{-11}

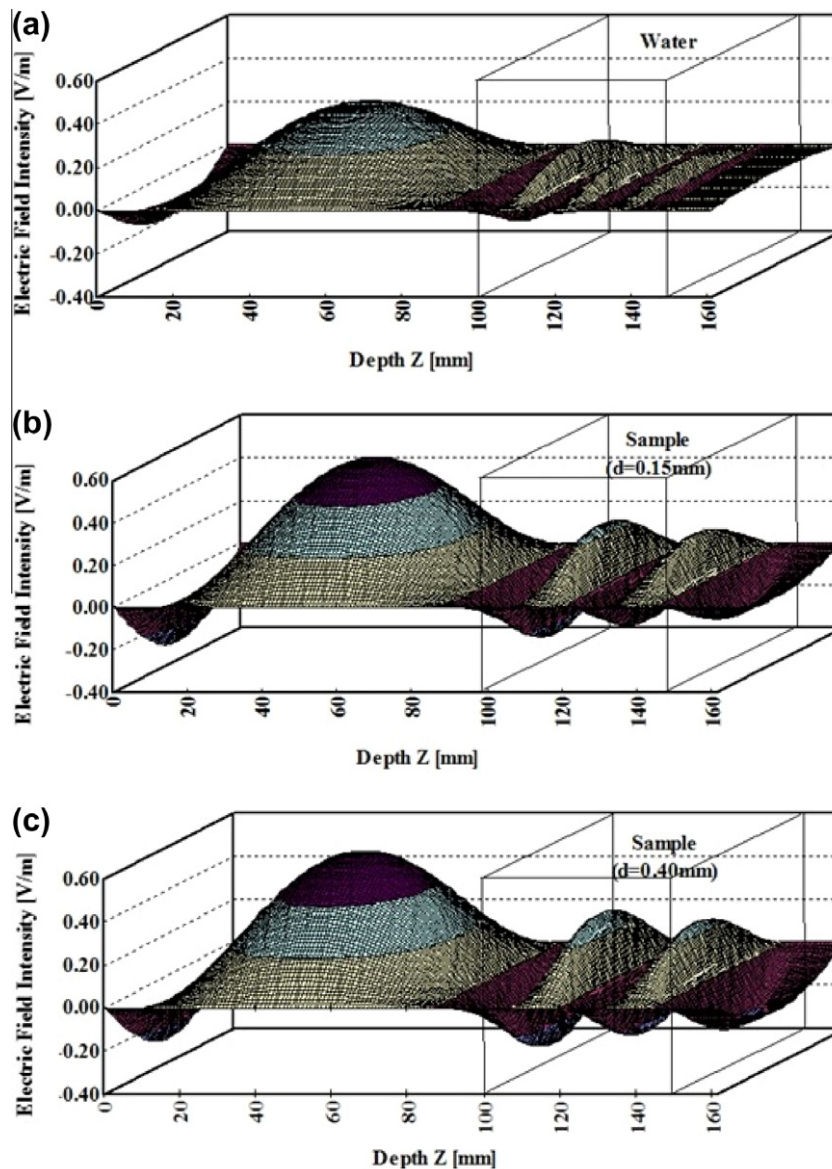


Fig. 3. Electric field distribution inside waveguide; (a) water layer; (b) saturated packed bed ($d = 0.15$ mm); (c) saturated packed bed ($d = 0.40$ mm).

intensity of the electric field in the TE_{10} mode is highest at the center region of the waveguide. Also, the temperature is higher closer to the surface of sample. In Fig. 4(a), water is a high lossy dielectric material and has a small penetration depth. Thus, the incident wave is decay rapidly. In Fig. 4(b) and (c), temperature is high at the middle of the packed beds and distributes to the wall. This is because of a standing wave that is formulated within packed beds.

Fig. 5(a) and (b) shows the comparison of temperature distribution between the simulated and experimental results along x and z axis, respectively. The comparison displays good agreement. Only small discrepancies are noticed. These may be resulted from keeping constant of some thermal properties during simulation process. For saturated packed bed, the experimental data are significantly higher than the computational results, especially along with x direction. The discrepancy may be attributed to uncertainties in some parameter such as porosity, (ϕ), the thermal and dielectric properties data base. Further, the uncertainty in temperature measurement might come from the error in measured microwave power input where the calculated uncertainty associated with temperature was less than 2.65%. Temperature inside packed beds

is higher than temperature inside a water layer (about 10 °C). Fig. 5(a), temperature is high at the center of the sample since the density of the electric field of the microwave in the TE_{10} mode is high around the center region of the waveguide. Fig. 5(b), the temperature is high at the surface and decreasing along the depth of the samples due to the penetration depth of microwave. The temperature of a packed bed having the particle size of 0.15 mm is higher than the temperature of the packed bed which has the particle size of 0.40 mm about 0.5 – 1.0 °C only. This is because the packed bed with small beads sizes has more amount of water in a pore than that a packed bed with the big glass beads sizes.

Flow patterns within the samples at $t = 60$ s are shown in Fig. 6. The flow patterns display in circulation patterns, which are characterized by the two symmetrical vortices. The fluid flows as it is driven by the effect of buoyancy. This effect is distributed from the upper corner near the surface where the incident wave propagates through. The buoyancy effect is associated with the lateral temperature gradient at locations near the top surface. Heated portions of the fluid become lighter than the rest of fluid, and are expanded laterally away from the center to the sides then flow down along

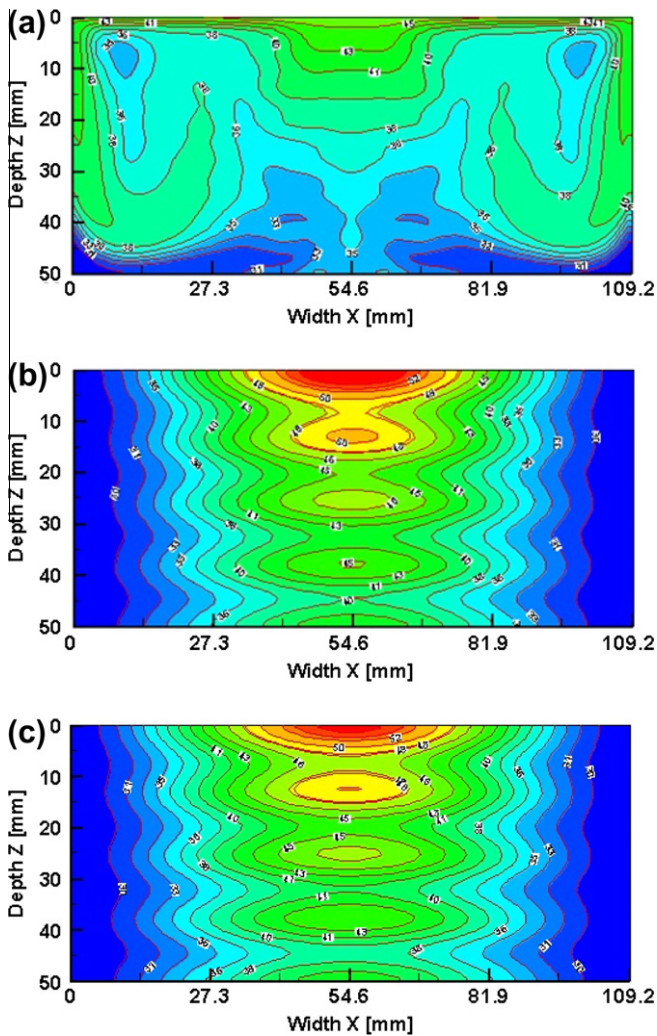


Fig. 4. Temperature profile within sample at $t = 60$ s; (a) water layer; (b) saturated packed bed ($d = 0.15$ mm); (c) saturated packed bed ($d = 0.40$ mm).

the two vertical walls, leading to the clockwise and counter-clockwise flow circulation. In addition, the permeability, κ of the porous medium (as seen in Table 3) has some effect on the fluid flow field within samples (Fig. 6(b) and (c)). The case in which the porous medium is absent corresponds to infinite permeability (Fig. 6(a)). The presence of packed beds has glass beads that resist the flow motions of the liquid in the voids. Comparing Fig. 6(b) and (c), it is shown that the increase in κ enhances the fluid flow intensities thereby assisting a flow penetration, which causes the stronger fluid flow. This results in expanding the region for which the convection significantly influences an overall heat transfer process. On the other hand, as the permeability decreases, the flow circulations as well as thermal penetration are progressively inhibited except at the region close to the location of convection surface condition where the flow motions are relatively strong. Furthermore, Fig. 6(b) indicates that low permeability, the convective heat transfer mechanism is almost suppressed, while the heat transfer by means of conduction plays an important role in heat transfer.

5.2. The effect of sample sizes

Fig. 7 displays temperature distributions within the packed beds with fine glass beads ($d = 0.15$ mm, $\phi = 0.385$) at various dimensions. The packed beds volume ($x \times y \times z$) that are chosen:

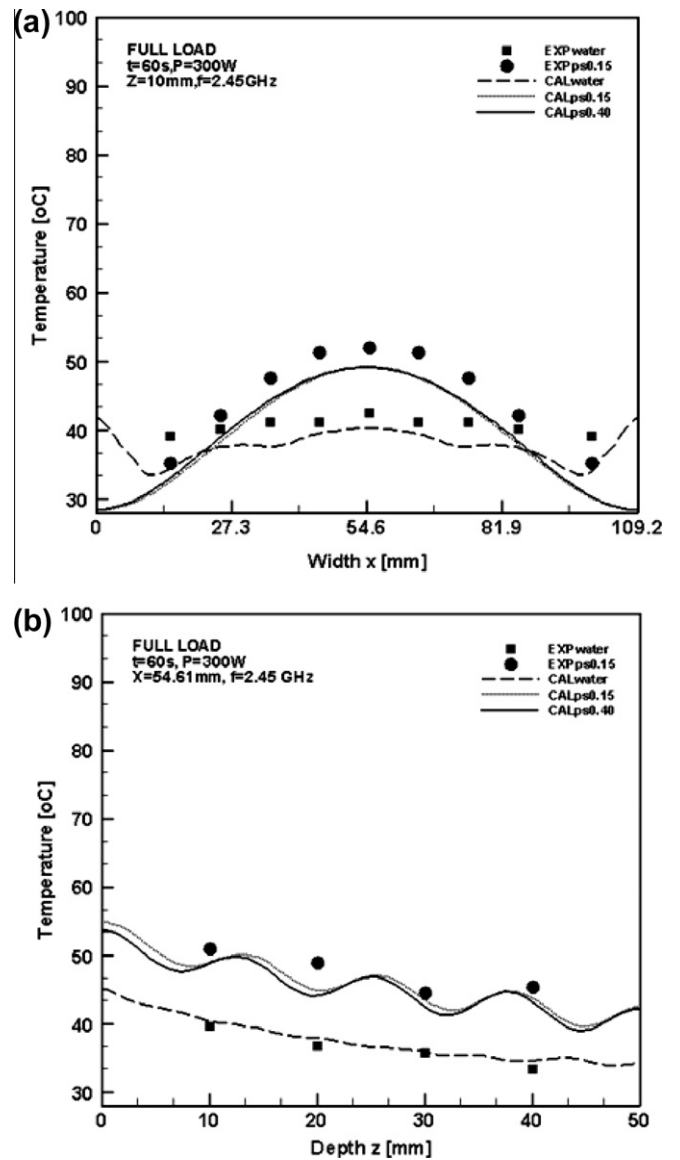


Fig. 5. Comparison of the temperature distribution between the simulated and experimental results within samples; (a) along x axis; (b) along z axis.

$109.22 \times 54.61 \times 30$ mm³, $109.22 \times 54.61 \times 40$ mm³, $109.22 \times 54.61 \times 50$ mm³ and $54.61 \times 54.61 \times 50$ mm³. The working frequency is 2.45 GHz. From the Fig. 7, temperature of the packed bed volume of $54.61 \times 54.61 \times 50$ mm³ is highest. The small volume is a higher rate of heat transfer than large volume due to larger heat generation rate per unit volume. However, the exception is observed that the packed bed with a dimension of $109.22 \times 54.61 \times 40$ mm³ is higher rate of temperature rise than the packed bed dimension of $109.22 \times 54.61 \times 30$ mm³. This is because the penetration depth effect causes the interference of waves reflected from the interface of the packed bed and air at the lower side. Consequently, the reflection and transmission components at each interface contribute to the resonance of standing wave inside the packed bed. Therefore the field distribution does not pass an exponential decay from the surface.

5.3. The effect of placement of sample inside a waveguide

This section examines the effect of placement of a partial packed bed ($54.61 \times 54.61 \times 50$ mm³) inside the rectangular

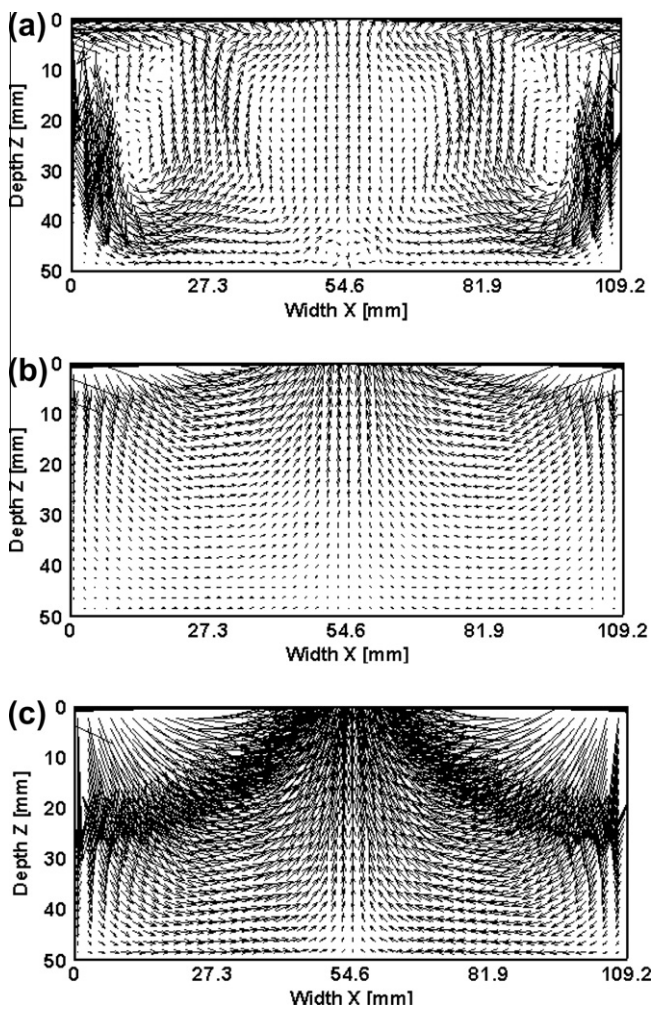


Fig. 6. Velocity field within sample at $t = 60$ s; (a) water layer; (b) saturated packed bed ($d = 0.15$ mm); (c) saturated packed bed ($d = 0.40$ mm).

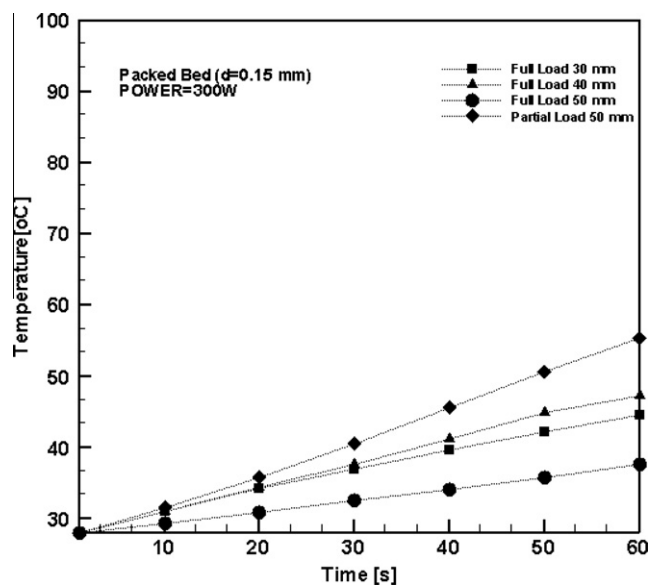


Fig. 7. Temperature distribution within the saturated packed bed ($d = 0.15$ mm) at various sizes.

waveguide on electric field distribution, temperature profile and a flow pattern. The investigated positions of sample are s0 and s20 as

shown in Fig. 2(a) and (b). The fine bead with diameter of 0.15 mm and the porosity of 0.385 is chosen to study in this subsection.

Fig. 8(a) and (b) exhibits the influence of placement of samples inside the waveguide on electric field distribution. The electric field is strength inside the packed bed and is symmetrical when a packed bed is placed at middle of the waveguide (s0). However, when a packed bed is moved from the center of 20 mm (s20), the wave pattern is drastically changed. This is because the effect of standing wave that is formulated at the walls.

Fig. 9(a) and (c) show the temperature profiles within a packed bed at $t = 60$ s with various placements inside the guide. The electric fields are consistent with temperature profiles. Fig. 9(a), temperature profile is symmetrical and similar to the case of full load ($109.22 \times 54.61 \times 50$ mm³). In the upper region of heating, temperature is relatively high and decreasing towards the lower boundary. Fig. 9(c), temperature profile is not symmetrical. The temperature distributes from the corners of the packed bed towards the lower side. In addition, it is interesting that the rate change of temperature becomes greatest when the sample is displaced 20 mm from the center. This result is attributed to the size of the sample that is smaller than the waveguide; therefore, waves reflect disorderly resulting in a multimode of field pattern.

Velocity fields within the packed bed on x - z plane in the microwave heating system are shown in Fig. 9(b) and (d). Several circulation patterns are observed. When a placement of the sample is shifted to 20 mm away from the center, there appears the transition from several circulations to one larger circulation pattern. The vectors are rigorous near the upper right corner. The velocity fields have a trend corresponding to that of temperature profiles.

5.4. The effect of microwave frequency

The last section discusses the effect of microwave frequency. The investigated microwave frequencies are 1.5, 2.45 and 5.8 GHz. These frequencies are chosen to show microwave heating phenomena because there are in set of frequencies reserved for industrial, scientific, and medical (ISM band) use. Besides the TE₁₀ mode, frequency of 5.8 GHz can propagate in both TE₂₀ and TE₀₁ modes since this frequency is above the frequency cutoff (2.75 GHz). Thus, the results below are just shown only for TE₁₀ mode. The packed bed volume is $109.22 \times 54.61 \times 50$ mm³ with fine beads ($d = 0.15$ mm) and the porosity of 0.385.

Fig. 3(b) and (c) shows the electric field distribution inside a rectangular waveguide when the porous packed bed is inserted inside the guide during microwave heating with the frequency of 2.45 GHz. Since the typical depth of packed bed is close to the penetration depth of microwave (as seen in Table 2), so a large part of microwaves are able to penetrate through the sample. The reflected wave will occur on each interface, from air (cavity) to upper surface and from lower surface of sample to air (cavity). The reflection and transmission components at each interface will contribute to the resonance of standing wave configuration inside the sample and give rise to a microwave absorption peak further from the surface exposed to incident microwaves. Thereafter the absorbed energy is converted to the thermal energy, which increases the sample temperature.

Fig. 10(a) shows the electric field distribution inside a rectangular waveguide when the porous packed bed is inserted inside the waveguide during microwave heating with the frequency of 1.5 GHz. The penetration depth of microwave is higher than the typical depth of a packed bed (as seen in Table 2), thus a majority of microwaves can penetrate and transmit from the sample. The absorbed waves are a little and slightly convert to the thermal energy. Fig. 10(b) shows the electric field distributions inside a rectangular waveguide when the porous packed bed is inserted in the waveguide during microwave heating with the frequency of

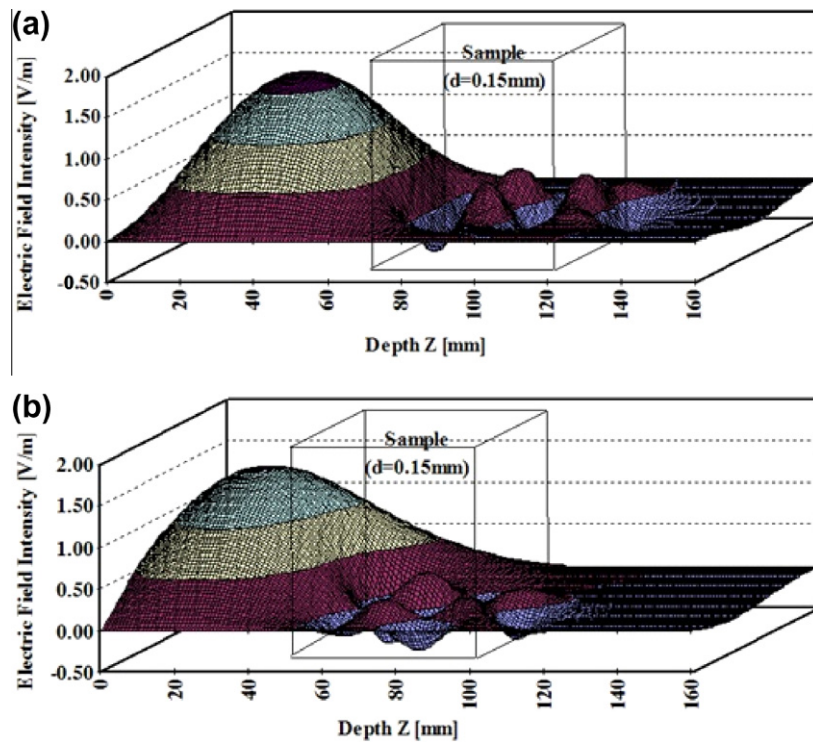


Fig. 8. Electric field distribution inside waveguide at various positions; (a) s0; (b) s20.

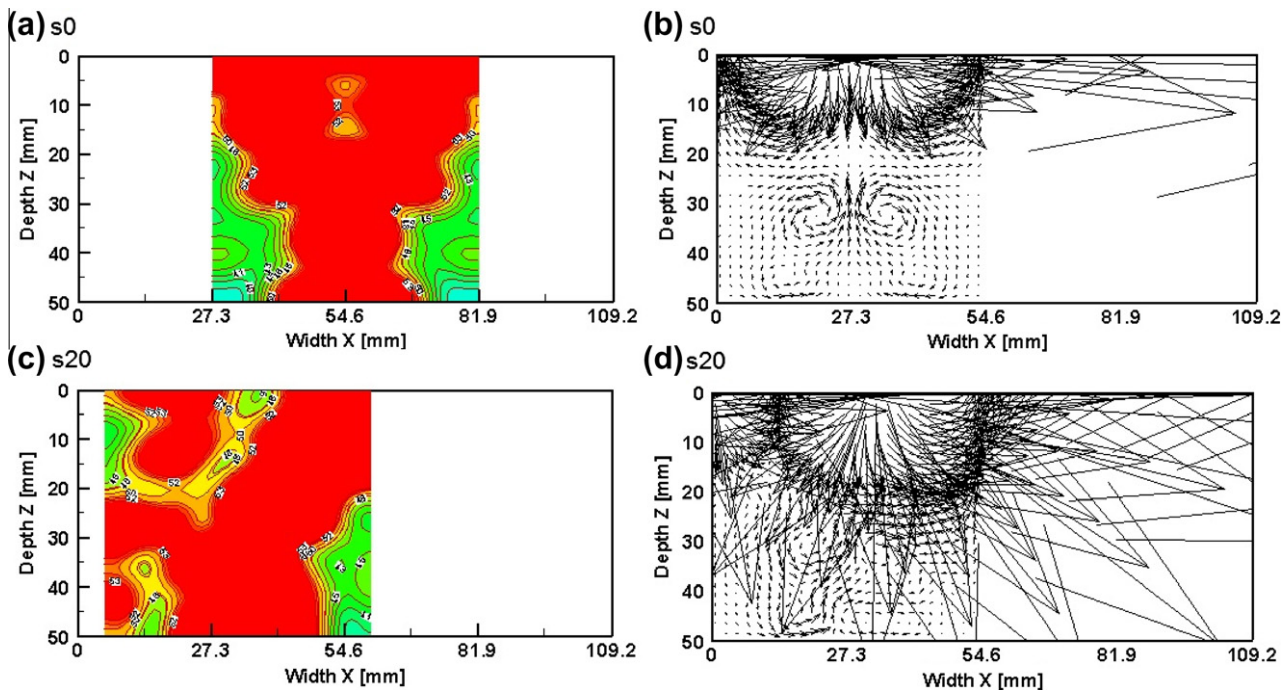


Fig. 9. Temperature profile and velocity field within a partial saturated packed bed ($d = 0.15$ mm) at $t = 60$ s; (a, b) s0; (c, d) s20.

5.8 GHz. In contrast to the electric field configuration in case 1.5 and 2.45 GHz, this is a result of a transmitted wave at the incident face and a reflected wave from the lower surface of the sample. This is due to the fact that microwave operating at a high frequency has a short wavelength which corresponds to a smaller penetration depth of microwave (as seen in Table 2) as compared with the depth of sample. Consequently, all microwaves, except the reflected waves from the upper surface of the sample, are absorbed by the sample.

Figs. 4 and 11(a) and (c) show the temperature profiles within the porous packed bed at the microwave frequencies of 2.45, 1.5 and 5.8 GHz, respectively. The temperature profile within the sample displays a wavy behavior corresponding to the resonance of electric field. This is because the electric field within the sample attenuates owing to energy absorption, and thereafter the absorbed energy is converted to the thermal energy, which increases the sample temperature. Since the higher microwave frequency (5.8 GHz) leads to a much smaller penetration depth and the

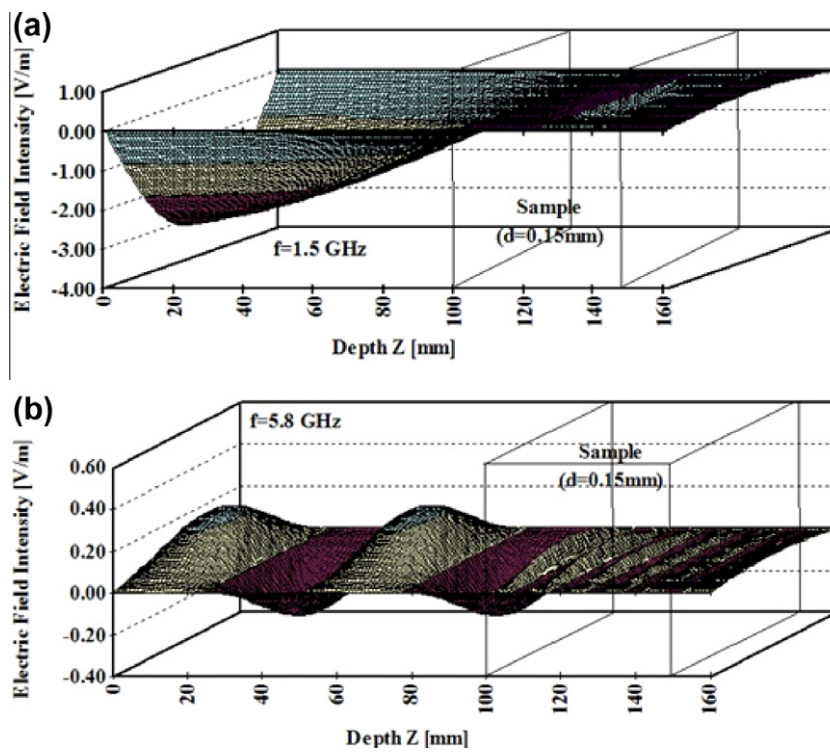


Fig. 10. Electric field distributions inside the waveguide at various microwave frequency; (a) 1.5 GHz; (b) 5.8 GHz.

electric field decays much faster as compared to that in the other cases of microwave frequencies. The microwave that operates at a high frequency has a short wavelength which corresponds to a smaller penetration depth of microwave (as seen in Table 2) compared with the depth of sample. Consequently, all microwaves, except the reflected wave from the upper surface of the sample, are absorbed by the sample. Therefore the microwave power absorbed

are the greatest at the surface exposed to the incident microwaves, and decay exponentially along the propagating direction with a very small wavelength, resulting in a thinner thermally stratified layer (as seen in Fig. 11(c)).

Figs. 6 and 11(b) and (d) depict the flow patterns within the packed beds at microwave frequencies of 2.45, 1.5 and 5.8 GHz, respectively. Fluid flow fields are displayed in the same direction

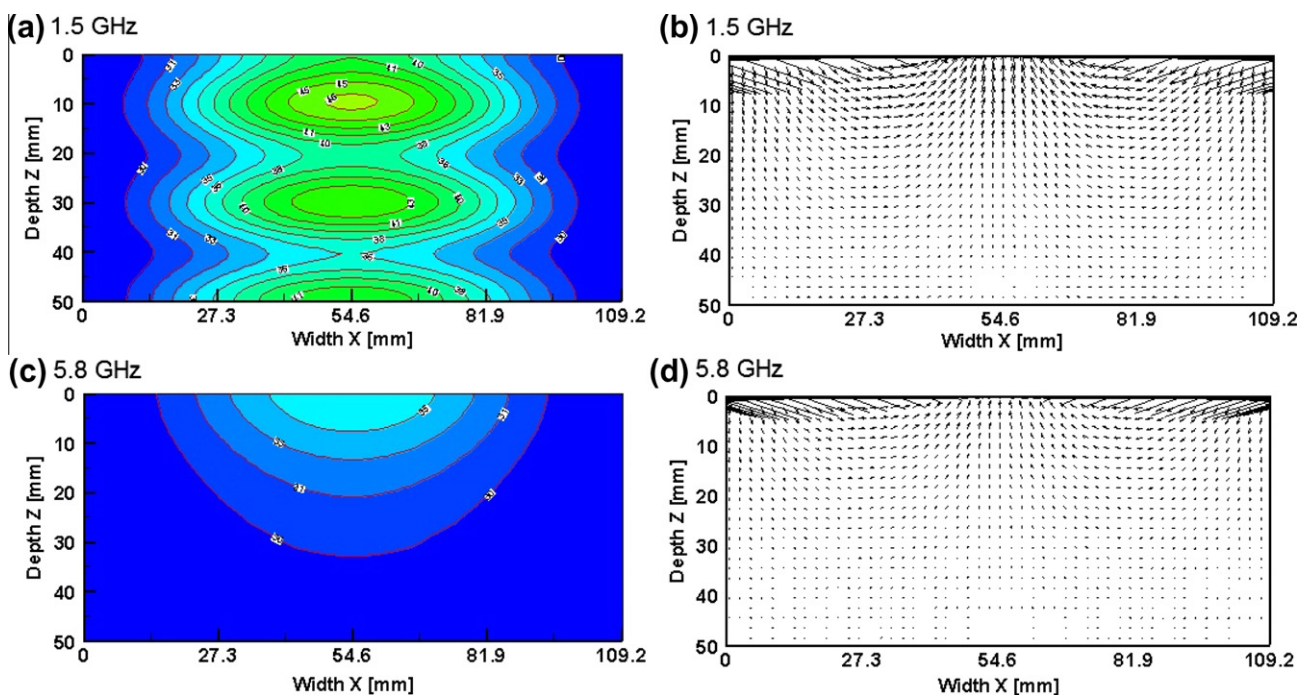


Fig. 11. Temperature profile and velocity field within a saturated packed bed ($d = 0.15$ mm) at $t = 60$ s; (a, b) 1.5 GHz; (c, d) 5.8 GHz.

but the magnitudes of flows are clearly different. The explanation of flow behaviors is similar discussed in the section of the effect of particle size.

For this research, porous packed beds are consisted of glass beads and water. It is noted that when the microwave frequency is changed, the dielectric properties of water layer will be changed corresponding to its frequency. Since the proposed model does not take into account for the change in the dielectric properties with microwave frequency (in this work refer to the dielectric properties of 2.45 GHz). Therefore, the error will occur in the cases of 1.5 and 5.8 GHz. However, the heating process is carried on a very short heating time (60 s), thus, the error arisen is minimal.

6. Conclusions

The numerical and experimental analysis presented in this work describes many of the interesting interactions within saturated porous medium during microwave heating. The following summarizes the conclusions of this work:

- (1) The mathematical model of heating of porous materials by microwave with a rectangular waveguide (TE_{10} mode) is purposed. This model is used successfully to explain the heating phenomena under the various conditions.
- (2) The results are shown that the changing glass bead size changes significant the flow pattern within the packed bed and the small beads higher generate energy absorbed than the large beads.
- (3) The high temperature depends on the optimum conditions (sample size, frequency) and the middle place of the waveguide results in the uniform heating of the packed bed.
- (4) The heat transfer by conduction plays an important role in microwave heating in porous packed bed.

Acknowledgement

The authors gratefully acknowledge the financial support this work provided by Thammasat University and the Thailand Research Fund (TRF) under the Royal Golden Jubilee Ph.D. Program (RGJ) Contract No. PHD/0201/2550.

References

- [1] C.A. Metaxas, R.J. Meredith, *Industrial Microwave Heating*, Peter Peregrinus, Ltd., London, 1983.
- [2] D.A. Nield, A. Bejan, *Convection in Porous Media*, Springer, New York, 1999.
- [3] P. Cheng, Heat transfer in geothermal systems, *Adv. Heat Transfer* 4 (1978) 1–105.
- [4] P.H. Oosthuizen, H. Patrick, *Natural Convection in an Inclined Square Enclosure Partly Filled with a Porous Medium and with a Partially Heated Wall*, HTD 302, American Society of Mechanical Engineers, Heat Transfer Division, 1995. pp. 29–42.
- [5] P. Nithiarasu, K.N. Seetharamu, T. Sundararajan, Natural convective heat transfer in a fluid saturated variable porosity medium, *Int. J. Heat Mass Transfer* 40 (16) (1997) 3955–3967.
- [6] P. Nithiarasu, K.N. Seetharamu, T. Sundararajan, Numerical investigation of buoyancy driven flow in a fluid saturated non-Darcian porous medium, *Int. J. Heat Mass Transfer* 42 (7) (1998) 1205–1215.
- [7] K.M. Khanafar, A.J. Chamkha, Mixed convection flow in a lid-driven enclosure filled with a fluid-saturated porous medium, *Int. J. Heat Mass Transfer* 42 (13) (1998) 2465–2481.
- [8] A.M. Al-Amiri, Analysis of momentum and energy transfer in a lid-driven cavity filled with a porous medium, *Int. J. Heat Mass Transfer* 43 (2000) 3513–3527.
- [9] W. Pakdee, P. Rattanadecho, Unsteady effects on natural convective heat transfer through porous media in cavity due to top surface partial convection, *Appl. Therm. Eng.* 26 (17–18) (2006) 2316–2326.
- [10] W. Chen Kou, H.T. Davis, E.A. Davis, Joan Gordan, Heat and mass transfer in water-laden sandstone: microwave heating, *AIChE J.* 31 (5) (1985) 842–848.
- [11] P. Rattanadecho, K. Aoki, M. Akahori, Influence of irradiation time, particle sizes, and initial moisture content during microwave drying of multi-layered capillary porous materials, *J. Heat Transfer* 124 (1) (2002) 151–161.
- [12] P. Rattanadecho, The simulation of microwave heating of wood using a rectangular wave guide: influence of frequency and sample size, *Chem. Eng. Sci.* 61 (2006) 4798–4811.
- [13] W. Cha-um, W. Pakdee, P. Rattanadecho, Experimental analysis of microwave heating of dielectric materials using a rectangular wave guide (MODE: TE_{10}) (Case study: water layer and saturated porous medium), *Exp. Therm. Fluid Sci.* 33 (3) (2009) 472–481.
- [14] H. Ni, A.K. Datta, K.E. Torrance, Moisture transport in intensive microwave heating of biomaterials: porous media model, *Int. J. Heat Mass Transfer* 42 (1999) 1501–1512.
- [15] D.D. Dinčov, K.A. Parrot, K.A. Pericleous, Heat and mass transfer in two-phase porous materials under intensive microwave heating, *J. Food Eng.* 65 (2004) 403–412.
- [16] T. Basak, A. Meenakshi, Influence of ceramic supports on microwave heating for composite dielectric food slabs, *AIChE J.* 52 (6) (2006) 1995–2007.
- [17] H. Zhang, A.K. Datta, I.A. Taub, C. Doona, Electromagnetics, heat transfer, and thermokinetics in microwave sterilization, *AIChE J.* 47 (9) (2001) 1957–1968.
- [18] P. Salagnac, P. Glouannec, D. Lecharpentier, Numerical modeling of heat and mass transfer in porous medium during combined hot air, infrared and microwave drying, *Int. J. Heat Mass Transfer* 47 (2004) 4479–4489.
- [19] P. Rattanadecho, K. Aoki, M. Akahori, A numerical and experimental investigation of the modeling of microwave heating for liquid layers using a rectangular wave guide (effects of natural convection and dielectric properties), *Appl. Math. Model.* 26 (2002) 449–472.
- [20] S.V. Patankar, *Numerical Heat Transfer and Fluid Flow*, Hemisphere, New York, 1980.
- [21] G. Mur, Absorbing boundary conditions for the finite-difference approximation of the time-domain electromagnetic-field equations, *IEEE Trans. Electromagn. Compat.* 32 (4) (1981) 377–382.